Rectification of Terrain Induced Distortions in Radar Imagery

Ronald Kwok, John C. Curlander, and *Shirley S. Pang*
Jet Propulsion Laboratory, California Institute of Technology, Pasadena, CA 91109

ABSTRACT: This paper describes a technique to generate geocoded synthetic aperture radar (SAR) imagery corrected for terrain induced geometric distortions. This algorithm transforms the raw slant range image, generated by the signal processor, into a map registered product, resampled to either Universal Transverse Mercator (UTM) or Polar Stereographic projections, and corrected for foreshortening. The technique utilizes the space platform trajectory information in conjunction with a digital elevation map (DEM) of the target area to generate an ortho-radar map with near-autonomous operation. The current procedure requires only two to three tie-points to compensate for the platform position uncertainty that results in translational error between the image and the DEM. This approach is unique in that it does not require generation of a simulated radar image from the DEM or a grid of tie-points to characterize the image-to-map distortions. Rather, it models the inherent distortions based on knowledge of the radar data collection characteristics, the signal Doppler parameters, and the local terrain height to automatically predict the registration transformation. This algorithm has been implemented on a minicomputer system equipped with an array processor and a large random-access memory to optimize the throughput.

INTRODUCTION

A TYPICAL side-looking radar design measures only the absolute sensor-to-target distance and samples the echo data at uniform intervals. The result is an image that in near range appears compressed with respect to far range. Furthermore, any deviation of the target elevation from a smooth geoid results in additional local distortions known as foreshortening and layover (Lewis, 1970). Radar foreshortening is the effect of imaged terrain surfaces sloping towards the radar appearing shortened relative to those sloping away from the radar. Radar layover is an extreme case of foreshortening that occurs when the slope of the terrain is greater than the angle of the incident signal. Although the slant-plane to ground-plane corrections can be predicted if the imaging geometry is known, the removal of the distortions due to target elevation requires an independent source of information either from a second imaging angle (stereo or interferometry) or surface topographic information.

In the absence of a second imaging angle, an essential element for the characterization of the local distortions in radar imagery is the availability of digital elevation maps (DEMs). Several techniques for image rectification of terrain distortion using DEMs have appeared in the literature (Naraghi, 1983; Domik, 1986); however, these methods depend on the relative registration of the radar image to a simulated image generated from the DEM using known imaging geometry. The procedure then requires a fine grid of tiepoints on the actual and simulated images to estimate the polynomial coefficients of a warping function that spatially transforms the radar image coordinates into the simulated image coordinates. Following co-registration, the radar image is resampled into a rectified format using the known distortions in the simulated image. Both the acquisition of the tiepoints and the generation of the simulated images are operator and computationally intensive processes. Because the resampling accuracy is directly a function of the tiepoint density, this technique is typically used only for small image frames.

This paper describes a procedure for rectification of terrain distortions employing only two to three tiepoints for a long image strip (up to 1000 km) that is more efficient than previous techniques because it eliminates the need for generation of an intermediate simulated radar image. These few tiepoints (in conjunction with their elevation) are used only to remove the residual translational errors between the predicted geodetic location of the target and its actual geodetic location on a topographic map. If terrain effects are absent, the geocoded radar image is inherently co-registered with the map base because these images are produced in the same grid system as the topographic maps. If there exists significant relief in the image, the imaging geometry and the DEMs are used to generate the transformation map which removes the local distortions when the slant range image pixels are spatially mapped into geocoded pixel locations.

This technique can be interfaced directly with the output of the synthetic aperture radar (SAR) image formation processor to produce these corrected images on the large scale, operational basis required by free-flying satellite SARs such as ERS-1, RADARSAT, JERS-1, and the planned polar platform (EOS) SAR. In addition, if the platform position uncertainty is reduced to less than a resolution cell such as is anticipated with the advent of onboard Global Positioning System (GPS) receivers, the need to perform any generation of tiepoints is eliminated and the process can be completely automated. The next section of this paper provides the theoretical basis for the rectification of terrain distortions in SAR imagery using DEMs. The operational procedures are described in the third section of this paper, followed by a description of the hardware and software environment of the rectification process in the fourth section. A summary of the results using SEASAT and SIR-B data and illustrations of geocoded images are shown in the fifth section with concluding remarks given in the final section.

THEORETICAL OVERVIEW

GEODETIC LOCATION OF SAR IMAGE PIXELS

A key element in the rectification procedure is an automated technique for precise determination of the geodetic location of an arbitrary slant range image pixel within an image frame using as input only the sensor position, the radar data collection parameters, and the image processing parameters. This technique, which has been previously described (Curlander, 1982), involves the simultaneous solution of three equations for the geocentric position $\mathbf{R}_t \epsilon (x_t, y_t, z_t)$ of a target. These three equations are:

Earth Model Equation. The shape of the Earth is approximated by an oblate ellipsoid:

$$\frac{x_t^2 + y_t^2}{R_e^2} + \frac{z_t^2}{R_p^2} = 1 \qquad (1)$$

where R_e is the mean equatorial radius, $R_p = (1\text{-}1/f)R_e$, and f is the Earth flattening factor. The equatorial radius is adjusted for each target area according to its average deviation from a precise geoid model.

PHOTOGRAMMETRIC ENGINEERING AND REMOTE SENSING,
Vol. 53, No. 5, May 1987, pp. 507–513.

0099-1112/87/5305–507$02.25/0

SAR Doppler Equation. The Doppler centroid of a target is approximated by

$$f_d = \frac{2}{\lambda R_{ij}}(\mathbf{V}_s - \mathbf{V}_t) \cdot (\mathbf{R}_s - \mathbf{R}_t) \quad (2)$$

where f_d is the Doppler parameter used in the azimuth phase reference function during image formation, λ is the radar wavelength, R_{ij} is the sensor-to-target slant range distance, $\mathbf{V}_s$ is the sensor velocity vector, $\mathbf{R}_s$ is the sensor position vector, and $\mathbf{V}_t$ and $\mathbf{R}_t$ are the target velocity and position vectors, respectively, with

$$\mathbf{V}_t = \boldsymbol{\omega}_e \times \mathbf{R}_t \quad (3)$$

where $\boldsymbol{\omega}_e$ is the Earth's rotational velocity.

SAR Range Equation. The slant range from the sensor to the target at a specific image pixel (i, j) is given by the vector product

$$R_{ij} = [(\mathbf{R}_s - \mathbf{R}_t).\ (\mathbf{R}_s - \mathbf{R}_t)]^{1/2}. \quad (4)$$

The simultaneous solution of Equations 1, 2, and 4 for the target position is performed numerically using an iterative process that first intersects the range vector with the geoid to determine a nominal target location and Doppler frequency. The range vector is then iteratively squinted by adjusting the platform attitude to intersect the appropriate iso-Doppler line given by f_d while maintaining the correct sensor-to-target range, R_{ij}.

In the absence of terrain effects, the above equations are sufficient to provide mapping of the image pixels onto a smooth geoid with sub-pixel internal distortion within an image frame.

Calculation of Target Displacement Due to Terrain Elevation

At any geodetic location, the displacement (due to elevation) of a target from its projected position on the geoid can be illustrated as in Figure 1. The slant range to target distance R_t can be expressed in terms of the sensor position $\mathbf{R}_s$ at the instant the target is imaged, and the geocentric location of the target $\mathbf{R}_{gt}$ by

$$R_t = |\ \mathbf{R}_{gt} - \mathbf{R}_s\ |$$

The range displacement of a target at an elevation h in the slant range image is given by

$$d = R_t(h) - R_t(0)$$

where $R_t(h)$ is the actual slant range distance to the target with geodetic height h and $R_t(0)$ is the slant range distance to the target orthogonally projected onto the geoid. With the above equation, the displacement of a target from its true geodetic location is calculated.

Tiepoint Acquisition and Refinement of Absolute Position of Sensor

The absolute geodetic location accuracy of an image pixel within an image frame is dependent on knowledge of the geocentric position and velocity of the sensor platform. The error in these parameters is highly correlated as a function of time and results in an along-track and cross-track bias in the absolute location of a target. These biases, which are measured using tiepoints, are used to correct the platform position by

$$\mathbf{R}_s = \mathbf{R}_s + \Delta\mathbf{r} \quad (5)$$

where $\Delta\mathbf{r}$ is the refinement to the platform position obtained from tiepointing. The refined position of the platform is then used to generate the transformation map described in the next subsection.

Transformation Map Generation

The simultaneous solution of Equations 1, 2, and 4 gives the geocentric location of an image pixel. The cartographic mapping of the image pixels is effected by mechanization of the appropriate equations (Snyder, 1983). The spatial relationship between the slant range-azimuth reference frame and the frame defined by the map grid in terms of coordinate transformations can be expressed as follows (Figure 2):

$$l = l(x',y') = l(x,y,\theta)$$
$$p = p(x',y') = p(x,y,\theta)$$

where (x,y) = coordinate frame defined by the map grid,
(x',y') = coordinate frame of the rectified image,
(l,p) = azimuth and range pixel location, and
(θ) = angle between grid north and y'.

The rectified image is in a grid defined by $x',y')$ where the

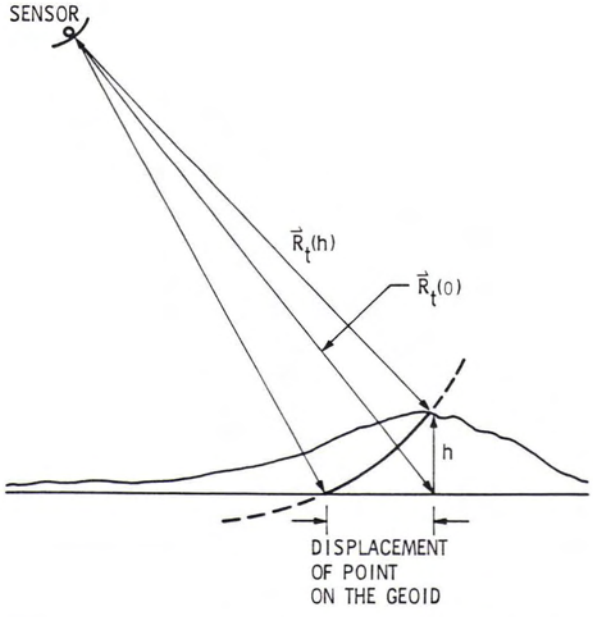

FIG. 1. Relief displacement of terrain features in radar images.

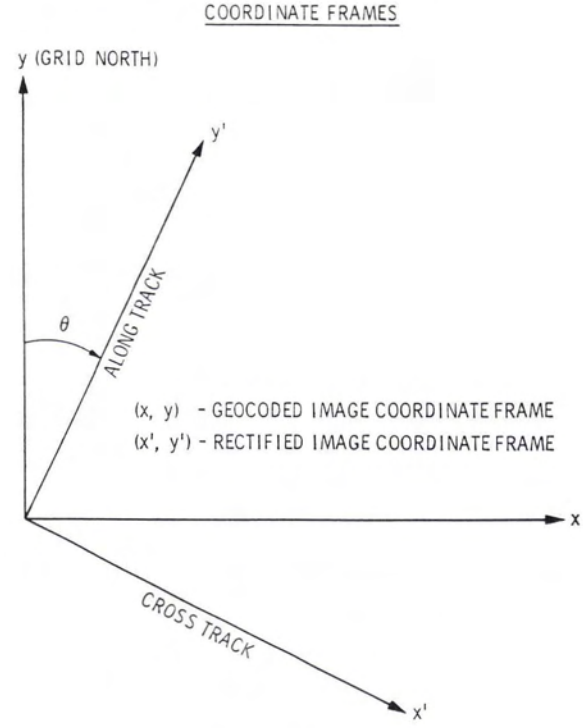

FIG. 2. Definition of coordinate frames.

abcissa (x') is parallel to the range direction and the ordinate (y') is parallel to the azimuth direction. A geocoded image is generated by the rotation and mapping of the rectified image into a grid defined by (x,y).

Three Pass Resampling — Geocoding with Rectification of Terrain Effects

A detailed description of the geocoding, rectification, and three-pass resampling processes can be found in Curlander *et al.* (1986). Following the generation of the transformation map, the slant range image is resampled into a geocoded format. Briefly, the three-pass resampling scheme is a combination of the rectification and rotation (both of which require two one-dimensional passes over an image) into a single three-pass process. The first pass rectifies the image in the azimuth dimension. Normally, the second pass is a rectification of the image in the range dimension and a vertical shear of the image. The rectification of the terrain distortion is inserted into this pass because it is primarily a range effect. A separate distortion map due to elevation is generated using digital terrain models. This map provides a pixel adjustment, given by

$$d_a = (R_t(h) - R_t(0))/dr$$

to each resampling location where dr is the slant range pixel spacing. The new resampling location then accounts for the cross-track displacement of a target. The third pass is final horizontal shear onto the geocoded grid.

PROCEDURE DESCRIPTION

A block diagram illustrating the rectification procedure is shown in Figure 3. Geocoded sub-images containing identifiable radar targets are generated using the techniques described in the previous section. To register the image to the DEM, the targets are located both on the image and on corresponding topographic maps. To minimize the error in map location of the targets, only high precision (1:24,000) U.S. Geological Survey (USGS) maps were used in the evaluation. The geodetic height of the targets (obtained from USGS digital terrain models) are used to remove the distortion due to target elevation. The location errors of the targets (after removal of terrain distortions) are used to estimate the position error of the platform. Usually, two to three tiepoints are sufficient to give a good approximation of these errors. Finally, a new geometric transformation map using the refined platform position is generated and the slant range image is three-pass resampled.

During the first pass, the slant range image is rectified and mapped in the azimuth dimension (see Figure 3). In the second pass, the distortion map containing the pixel adjustments necessary to account for relief displacement of each location is generated and combined with the resampling locations for a smooth geoid to produce the correct resampling location in the slant range image. The intermediate image from the first pass is then resampled in range and vertically sheared. Finally, in the third pass the intermediate image from the second pass is horizontally sheared into a geocoded format.

IMPLEMENTATION

The system architecture for geocoding and terrain correction is a subset of the overall system hardware utilized by the operational SAR correlator. This system is configured around a System Engineering Laboratory (SEL) 32/77 minicomputer with a Floating Point System (FPS) AP120B array processor, three CDC 300 Mbyte disks, and a 32 Mbyte Texas Memory Systems random access memory (RAM) with system interfaces to both the SEL and the array processor. The SEL, which acts as a host to the array processors, is equipped with 128 K words of 600 ns solid state memory. A block diagram of the system hardware configuration is shown in Figure 4. The input slant range image records, the digital elevation model, and the output geocoded

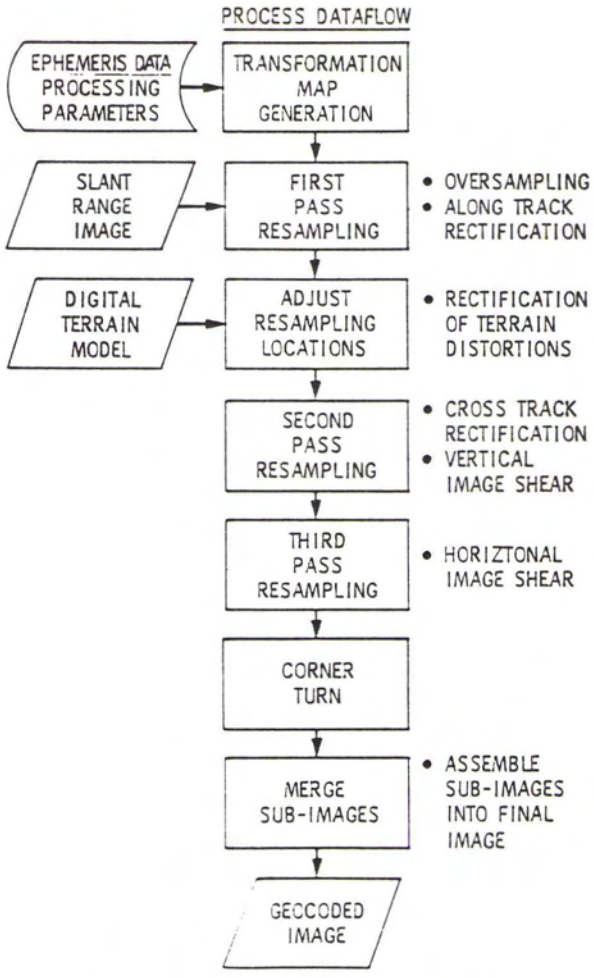

Fig. 3. Data flow of rectification process.

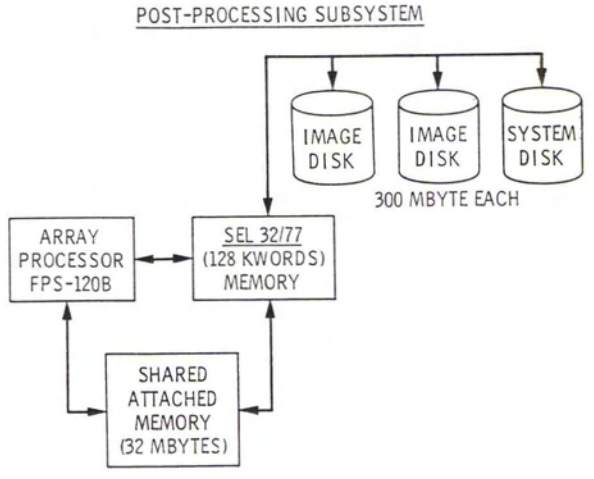

Fig. 4. System hardware configuration.

image records are stored in disk files common with the SAR processor output. The RAM serves as storage for the intermediate image from each resampling pass and is divided into two buffers: buffer 1 (20 Mbytes) is used to store the pass 1 output image and buffer 2 (12 Mbytes) is used to store the pass 2 output image. Data resampling is performed using a four point cubic spline interpolator. All resampling is performed in the array processor (AP). The sensor ephemeris data and the processor control parameters such as output image size, pixel spacing, and the center location are stored in a disk resident parameter

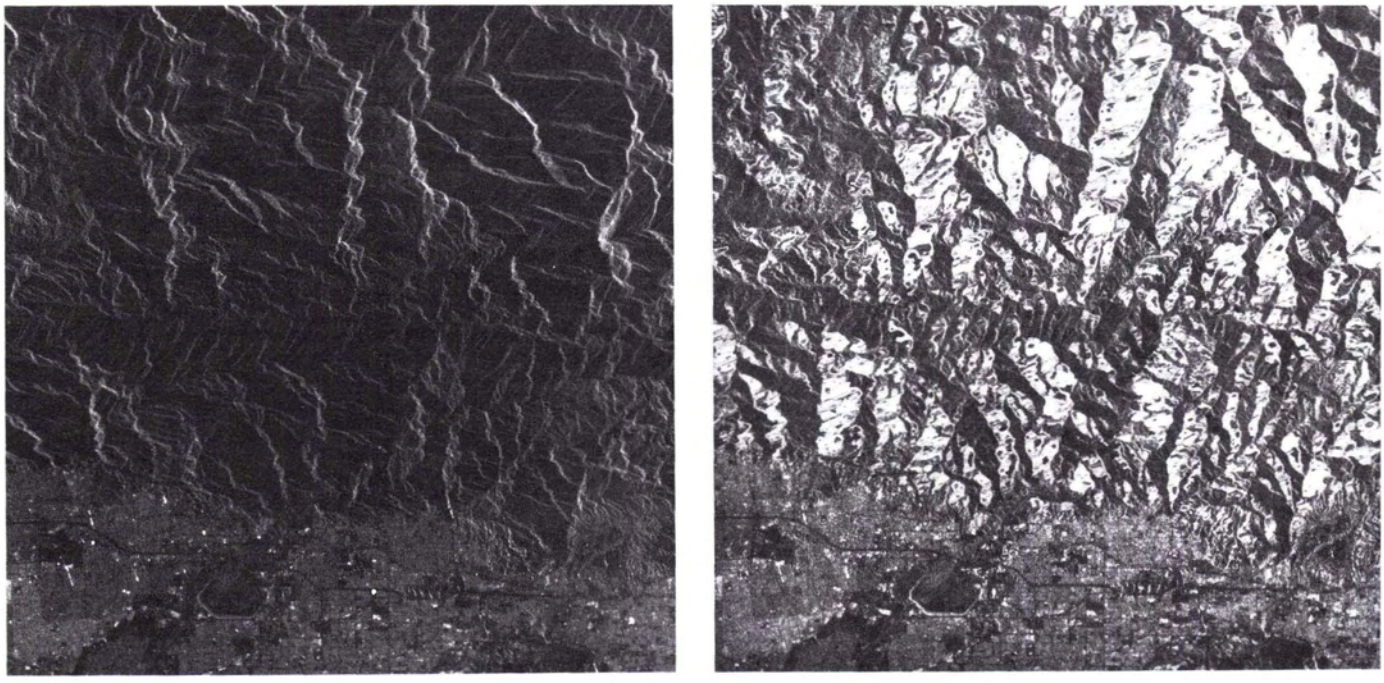

FIG. 5. SEASAT image of Los Angeles area - Ascending pass (Rev. 351) (2k by 2k pixels). (a) Geocoded image - UTM. (b) Geocoded image with correction of terrain effects.

TABLE 1. PROCESSING THROUGHPUT USING ONE AP

Mission	Output Image Size (pixels)	Processing Time(s)	
		Geocoding	Geocoding w/Terrain Rectification
SIR-B	1K by 1K	530	2400
SEASAT	1K by 1K	470	1700

TABLE 2. LOCATION ACCURACY OF SAR IMAGERY (AFTER TERRAIN RECTIFICATION)

Image Location	Number of Points	Azimuth Error(m)		Range Error(m)	
		$\bar{x}$	$\bar{\sigma}_x$	$\bar{y}$	$\bar{\sigma}_y$
SEASAT Rev 351	4	−4	27	−6	34
SEASAT Rev 416	4	9	28	−9	5

file that is automatically established by the SAR correlator during the initial image generation.

The processing algorithm for generation of the geocoded and terrain corrected SAR image consists of three modules which correspond to the three main processing steps: generation of the image transformation map, generation of the terrain correction map, and three pass resampling. The first step generates the correction data which provides the mapping of the slant range pixels into the output grid. Calculation of the interpolation and rotation coefficients (see second section) is done at this stage. The second step generates a table which maps the range pixels into their appropriate geodetic locations. This provides for the correction of the cross-track displacement of image features due to the effect of terrain. The third step performs the actual resampling of the image data. Due to the memory limitations of the post-processing system, the image data are divided, resampled in small blocks (1 K by 1 K pixels), and reassembled into the full image at the end of the correction process.

Operationally, the data flow in each resampling pass is very similar. Each image line goes through five discrete processing functions: (1) input from disk or the RAM, (2) data transfer to the AP, (3) calculation of the resampling locations, (4) resampling in the AP; and (5) transfer of the data from AP to disk. These functions are sequential in nature and mutually independent; therefore, an optimal approach utilizing concurrent execution with pipelined data flow is implemented.

Table 1 presents a throughput summary of these geocoding and terrain correction operations. The table shows the amount of time required for geocoding, and for geocoding with terrain correction. The main computational load is in generating the cross-track displacements of image features because these displacements are calculated for each range pixel. The throughput can be further improved by using multiple array processors and streamlining of the algorithms; both methods are currently being investigated.

RESULTS

The rectification procedure was tested using SEASAT and SIR-B imagery. Figures 5 and 6 are examples of the application of the process to a SEASAT radar image of an area north of Los Angeles. Figure 5 was an ascending pass (Rev 351) and Figure 6 (Rev 416) was a descending pass. Two images are displayed in each figure: (a) a geocoded (UTM) image without terrain correction, and (b) the radar image geometrically rectified to remove topographical effects. The terrain appears different because they were illuminated from opposite directions as shown in both figures. Because the rectified images have been previously geocoded, their geodetic accuracy can easily be checked with map tiepoints. Target features were selected from each terrain corrected image for this purpose. Table 2 shows the absolute location accuracy of these targets. The geodetic accuracy of the images demonstrate that geocoded multi-temporal imagery can be easily overlayed using this process. Figure 7 shows a comparison of a descending pass of a Landsat TM image (Band 4) with that of a terrain-rectified SEASAT image (descending pass) of the same area. After both images have been resampled to

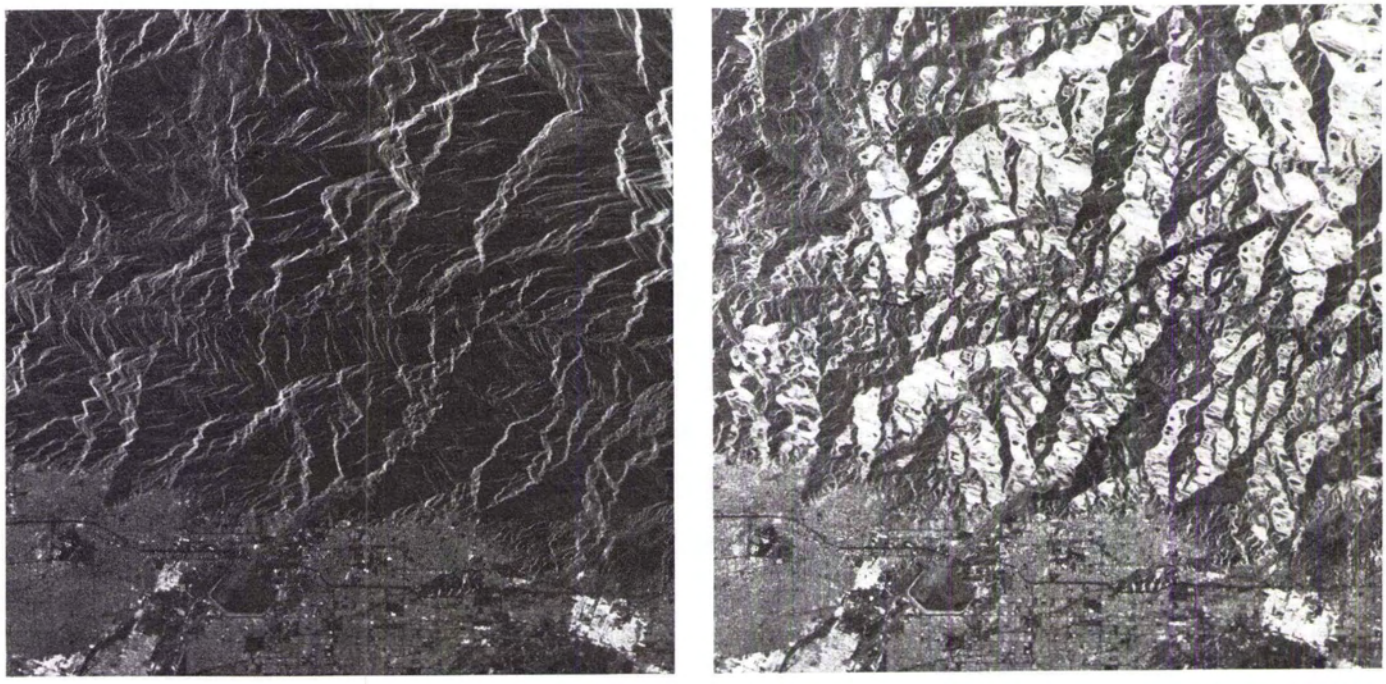

FIG. 6. SEASAT image of Los Angeles area - Descending Pass (Rev. 416) (2k by 2k pixels). (a) Geocoded image - **UTM**. (b) Geocoded image with correction of terrain effects.

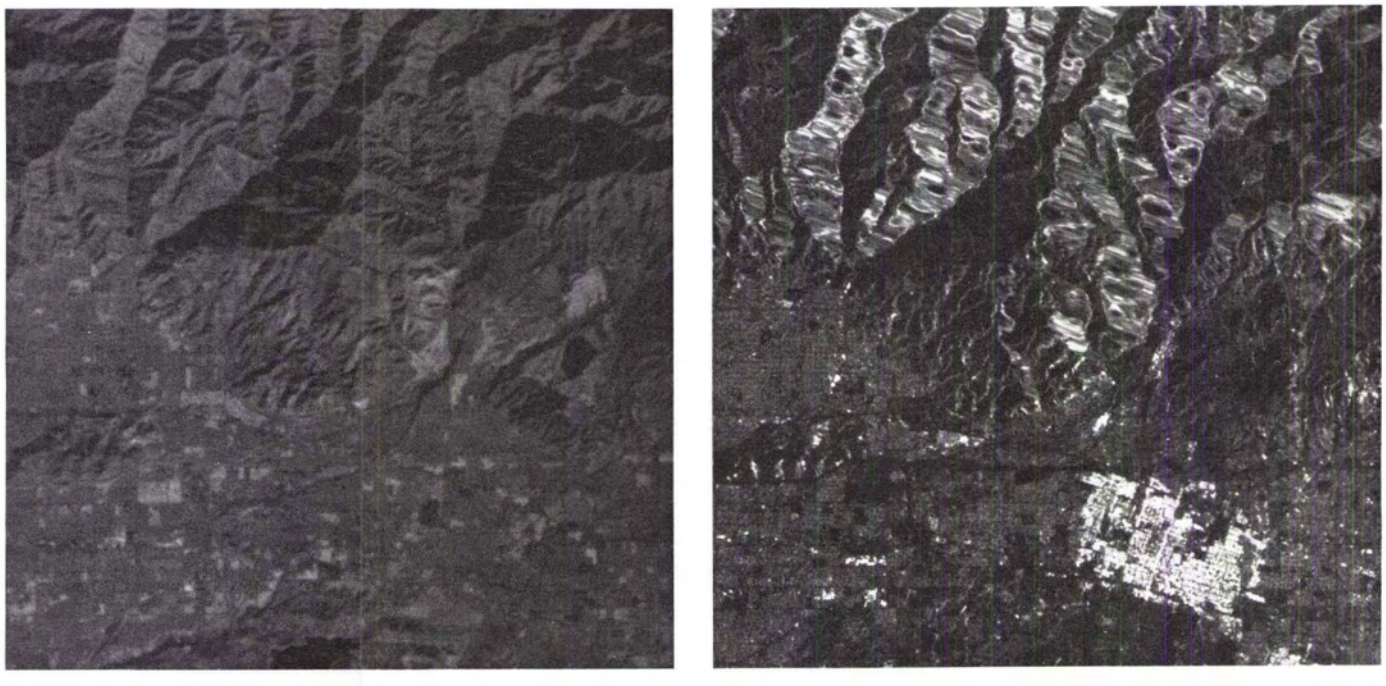

FIG. 7. Comparison of descending imaging passes of Landsat and SEASAT. (a) Geocoded Landsat **TM** (Band-4) image - **UTM**. (b) Goocoded **SEASAT** image (Rev. 416) - **UTM**.

the same pixel spacing they can be overlayed, demonstrating the utility of this geocoding with terrain correction procedure for analysis of data from different sensors.

Figure 8 shows the application of the rectification process to a SIR-B image of an area near Death Valley. Figure 8a is a geocoded image of the area and Figure 8b is the same area with the terrain distortions removed. The geometric effects of the corrected SIR-B image are not as dramatic as the SEASAT images because of the shallower incidence angle of the radar when this scene was imaged.

A mosaic of three SEASAT frames is shown in Figure 9. Each frame is geocoded (with correction of terrain distortions) independently and mosaicked together without tiepoints. Only the predicted coordinates were used to determine the locations of

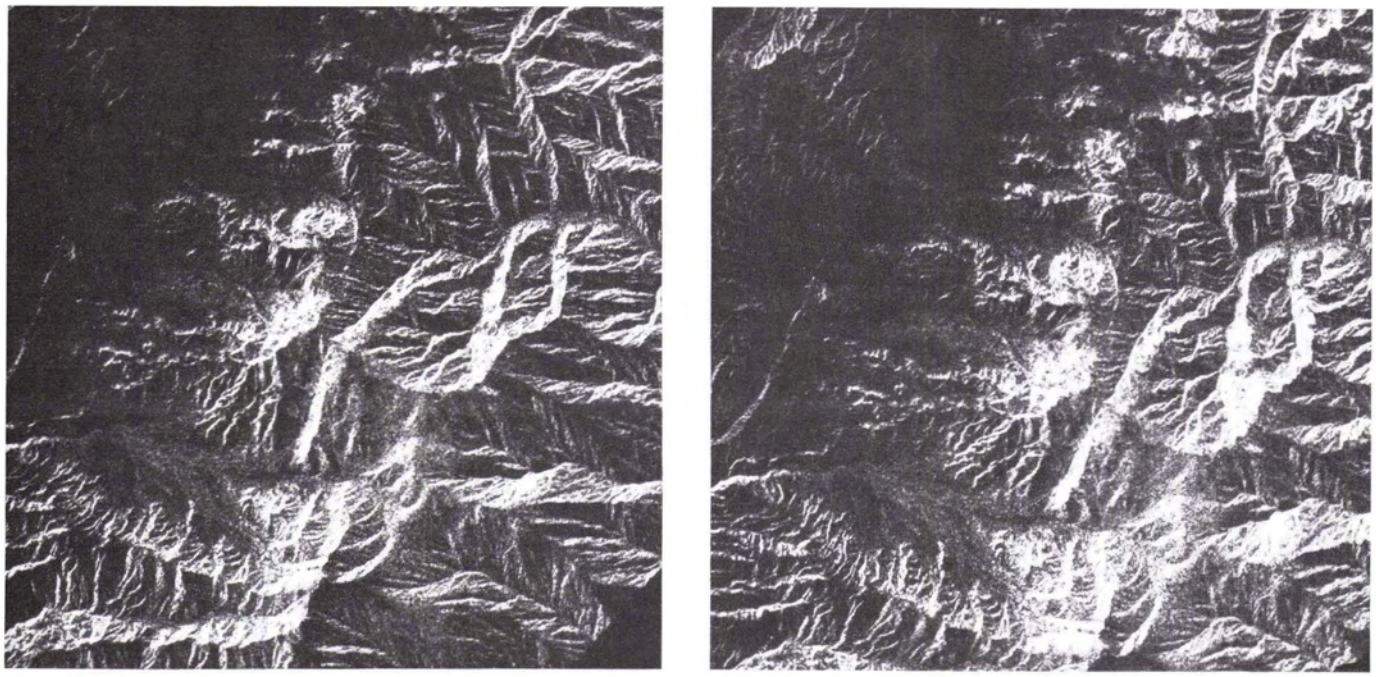

FIG. 8. SIR-B image of an area near Death Valley (lk by lk pixels). (a) Geocoded image - UTM. (b) Geocoded image with correction of terrain effects.

the overlaps, and no attempts were made to modify the radiometric values at the seams. With this technique, mosaics of larger areas could easily be generated automatically without operator interaction. Software for performing this automatic mosaicking is currently in the development stage.

DISCUSSION

The technique described in this paper for automated generation of terrain corrected geocoded imagery is an important step toward development of an end-to-end data system that is capable of delivering refined products to the user in near-real time. This algorithm produces imagery that can be directly registered to either a map base or image data from other sensors that are in an identical map coordinate system. The fact that this technique can be completely automated such that no operator interaction is required is key for future operational SAR systems that cannot afford to backlog data for later processing.

This procedure is unique in that it utilizes directly the raw image output from the digital SAR correlator to produce the map registered product. The geocoding and rectification procedures are performed in a single operation. The terrain correction has been integrated into this operation such that it does not require generation of intermediate image products. This approach results in an enhanced efficiency in terms of throughput for a given system architecture. An analysis of the final products by comparison with high precision maps has demonstrated that the accuracy of this technique is on the order of one resolution cell (25 m) or less.

Considering the large volume of image data that will be produced by the ERS-1 RADARSAT, J-ERS1, and EOS (polar platform) SAR, automated techniques for signal and image processing are needed to reduce, evaluate, and utilize the information contained in these data sets. To date, the bulk of the effort in SAR data processing has concentrated on reduction of the raw signal data to imagery. With the advent of custom dedicated SAR processors, which now exist or will exist at the major processing centers for NASA, ESA, NASDA, and RADARSAT, the bottleneck shifts downstream to the post-processing and image interpretation operations. The techniques described in this paper directly address the problem of transforming the raw image output of the signal processor (correlator) into a precision map registered product in an efficient automated fashion compatible with the new generation of SAR processors.

The challenge facing us now is how to reliably extract the information from these products (in conjunction with other types of correlative data) and deliver it to the end user in near-real time. Obviously, precise calibration of the input images to this geophysical processor responsible for image interpretation is a prerequisite. In addition, a wide-band communication network is needed for distribution of the resulting information to the user community. In between, an expert system capable of accessing data from a number of sources (remote data bases) must be developed that can derive from the SAR imagery the geophysical information for which it was acquired. This mandates a coordinated effort between the discipline scientists to define the required outputs and the data system engineers to implement these algorithms that deliver these outputs in an efficient automated fashion. This paper presents the groundwork for development of the geophysical processor by providing calibrated precision imagery routinely available for analysis.

ACKNOWLEDGMENT

The authors wish to thank S. Officer and J. Weirick for technical support and in the preparation of this manuscript. This work was carried out at the Jet Propulsion Laboratory, California Institute of Technology, under contract with the National Aeronautics and Space Administration.

REFERENCES

Curlander, J.C., 1982. Location of Spaceborne SAR Imagery, *IEEE Trans. Geoscience and Remote Sensing*, Vol. GE-20, 359.

———, , 1984. Utilization of Spaceborne SAR Data for Mapping, *IEEE Trans. Geoscience and Remote Sensing*, Vol. GE-22, 106

Curlander, J.C., R. Kwok, and S.S. Pang, 1986. A Post-Processing System for Automated Rectification and Registration of Spaceborne

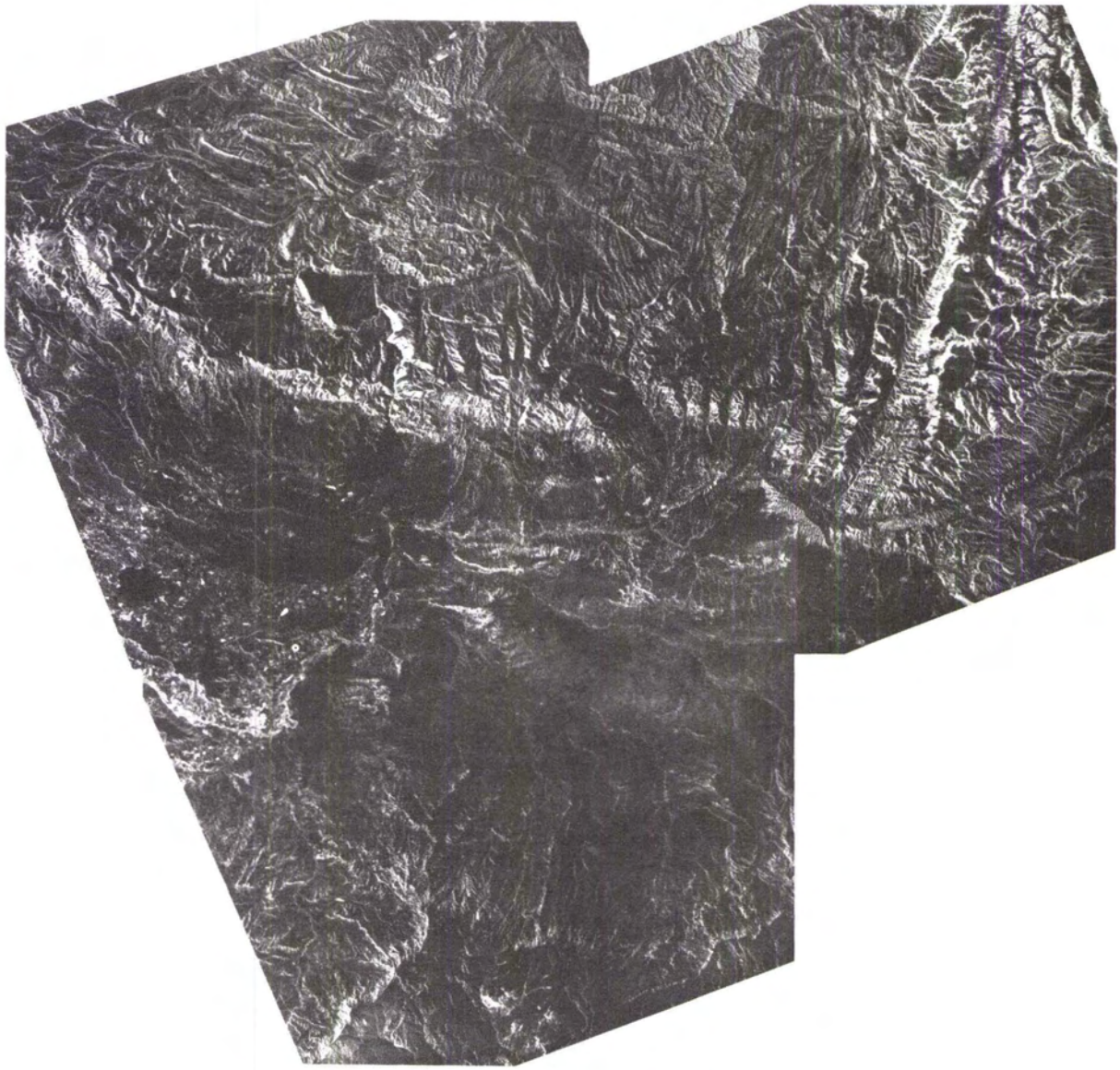

FIG. 9. Mosaic of three **SEASAT** frames of an area in Wyoming (**UTM** - 5.5k by 5.2k pixels).

SAR Imagery. To be published in the International Journal of Remote Sensing,

Domik, G., F. Leberl, and J.B. Cimino, 1986. Multiple Incidence Angle SIR-B Experiment Over Argentina: Generation of Secondary Image Products. *IEEE Trans. Geoscience and Remote Sensing*, Vol. GE-24, 492.

Lewis, A.J., and H.C. MacDonald, 1970. Interpretive and Mosaicking Problems of SLAR Imagery. *Remote Sensing of Environment*, 1, 231.

Naraghi, M., W. Stromberg, and M. Daily, 1983. Geometric Rectification of Radar Imagery Using Digital Terrain Models. *Photogrammetric Engineering and Remote Sensing*, Vol. 49, No. 2, 195.

Snyder, John P., 1983. *Map Projections Used by the U.S. Geological Survey*. Geological Survey Bulletin 1532.

(Received 8 December 1986; accepted 4 February 1987)

In Recognition

The American Society for Photogrammetry and Remote Sensing would like to thank and recognize Dr. Kevin P. Gallo for his contribution of time and effort in working during 1986 as a reviewer for the technical papers that appear in this Journal. We regret that his name was inadvertently omitted from the list of reviewers published in the January 1987 issue.